THE JOURNAL OF BIOLOGICAL CHEMISTRY VOL. 288, NO. 10, pp. 6835–6848, March 8, 2013

Thioredoxin-interacting Protein Mediates High Glucose-induced Reactive Oxygen Species Generation by Mitochondria and the NADPH Oxidase, Nox4, in Mesangial Cells*

Received for publication, September 12, 2012, and in revised form, January 16, 2013 Published, JBC Papers in Press, January 17, 2013, DOI 10.1074/jbc.M112.419101

Anu Shah[‡§¶‖1], **Ling Xia**[§‖], **Howard Goldberg**[§‖], **Ken W. Lee**[‡§¶‖2], **Susan E. Quaggin**[‡¶‖], **and I. George Fantus**[‡§¶‖3]

From the [‡]*Department of Medicine and Samuel Lunenfeld Research Institute, Mount Sinai Hospital,* [§]*Toronto General Research Institute, University Health Network, and the* [¶]*Department of Physiology and* [‖]*Banting and Best Diabetes Centre, University of Toronto, Toronto, Ontario M5T 3L9, Canada*

Background: Thioredoxin-interacting protein (TxNIP) is up-regulated by high glucose (HG), inhibits the antioxidant, thioredoxin, and thereby is implicated in oxidative stress.
Results: TxNIP deficiency protects mesangial cells from HG-induced oxidative stress and increased collagen by blocking mitochondrial glucose metabolism, NADPH oxidase, and Nox4.
Conclusion: TxNIP controls ROS generation by regulating the TCA cycle *versus* glycolytic glucose flux.
Significance: Inhibition of TxNIP is a promising approach to treat glucose toxicity.

Thioredoxin-interacting protein (TxNIP) is up-regulated by high glucose and is associated with oxidative stress. It has been implicated in hyperglycemia-induced β-cell dysfunction and apoptosis. As high glucose and oxidative stress mediate diabetic nephropathy (DN), the contribution of TxNIP was investigated in renal mesangial cell reactive oxygen species (ROS) generation and collagen synthesis. To determine the role of TxNIP, mouse mesangial cells (MC) cultured from wild-type C3H and TxNIP-deficient Hcb-19 mice were incubated in HG. Confocal microscopy was used to measure total and mitochondrial ROS production (DCF and MitoSOX) and collagen IV. Trx and NADPH oxidase activities were assayed and NADPH oxidase isoforms, Nox2 and Nox4, and antioxidant enzymes were determined by immunoblotting. C3H MC exposed to HG elicited a significant increase in cellular and mitochondrial ROS as well as Nox4 protein expression and NADPH oxidase activation, whereas Hcb-19 MC showed no response. Trx activity was attenuated by HG only in C3H MC. These defects in Hcb-19 MC were not due to increased antioxidant enzymes or scavenging of ROS, but associated with decreased ROS generation. Adenovirus-mediated overexpression of TxNIP in Hcb-19 MC and TxNIP knockdown with siRNA in C3H confirmed the specific role of TxNIP. Collagen IV accumulation in HG was markedly reduced in Hcb-19 cells. TxNIP is a critical component of the HG-ROS signaling pathway, required for the induction of mitochondrial and total cell ROS and the NADPH oxidase isoform, Nox4. TxNIP is a potential target to prevent DN.

Diabetic nephropathy (DN),[4] a microvascular complication of diabetes mellitus, is a major cause of morbidity and mortality resulting in end stage renal disease requiring dialysis and/or transplantation (1–3). Although chronic exposure to elevated levels of glucose is the central cause, the molecular pathogenesis remains to be completely defined (4). The pathological hallmarks of DN include increased mesangial matrix expansion associated with increased production and decreased degradation of extracellular matrix (ECM) proteins such as fibronectin, laminin, and collagen (2, 5–8).

A major link between high glucose and cellular dysfunction is oxidative stress (9, 10). Thus, it has been proposed that increased metabolic flux of glucose via mitochondrial glucose oxidation leads to the increased production of reactive oxygen species (ROS), such as O_2^- (superoxide), a byproduct of electron transport (9). ROS generation in excess of endogenous antioxidant neutralizing capacity leads to oxidative stress. This in turn leads to an inhibition of glyceraldehyde-3-phosphate dehydrogenase (GAPDH) activity, promoting increased flux through upstream glycolytic branch pathways, including the aldose reductase/polyol pathway, formation of reactive sugars and advanced glycation end products, *de novo* synthesis of diacylglycerol and chronic activation of PKCs, and increased intracellular *O*-glycosylation via the hexosamine biosynthetic pathway

* This work was supported in part by Canadian Institutes of Health Research Grants MOP 97979 and PCN 49409 (to I. G. F.).
[1] Supported in part by a Novo Nordisk Studentship from the Banting and Best Diabetes Centre, a Canada Graduate Scholarship (NSERC), and an Ontario Graduate Scholarship.
[2] Supported in part by a Novo Nordisk Studentship from the Banting and Best Diabetes Centre and Canadian Diabetes Association Grant OG-3–10–2997-IF.
[3] To whom correspondence should be addressed: Mount Sinai Hospital, 60 Murray St., Joseph and Wolfe Lebovic Building, Suite 5–028, Toronto, Ontario M5T 3L9, Canada. Tel.: 416-586-8665; Fax: 416-361-2657; E-mail: gfantus@mtsinai.on.ca.

[4] The abbreviations used are: DN, diabetic nephropathy; TxNIP, thioredoxin-interacting protein; ROS, reactive oxygen species; MC, mesangial cells; ECM, extracellular matrix; O_2^-, superoxide; SOD, superoxide dismutase; Trx, thioredoxins; DHE, dihyroethidium; MnSOD, manganese-dependent superoxide dismutase; HO-1, heme oxygenase-1; CM-H_2DCFDA, carboxymethyl-H_2-dichlorofluorescein diacetate; AdTxNIP, TxNIP expressing adenovirus; AdGFP, GFP expressing adenovirus; HG, high glucose; NG, normal glucose; ifu, infectious units.

(9, 10). At the same time, ROS have been shown to be increased in the presence of high glucose by activation of NADPH oxidases (11–16). *In vivo* studies of diabetic rodents demonstrate protection against complications by antioxidants, by inhibition of NADPH oxidase, and by genetic overexpression of antioxidant enzymes, such as Cu,Zn-superoxide dismutase (SOD) (17–19). More recently, *in vivo* and *in vitro* evidence for up-regulation by high glucose of NADPH oxidase subunits, *e.g.* $p22^{phox}$ and $p47^{phox}$, as well as the predominant renal isoform, Nox4, strongly support this concept (13–16, 20).

The importance of oxidative stress as a mediator of high glucose-induced pathology has led to studies of its regulation. One protein found to be markedly up-regulated by high glucose in a number of cells, including mesangial cells and pancreatic β-cells is thioredoxin-interacting protein (TxNIP), also known as vitamin D up-regulated protein 1 (VDUP1) (7, 21–24). TxNIP has been implicated in promoting oxidative stress by binding and inhibiting thioredoxins (Trx)-1 and -2, ubiquitous antioxidant oxidase-reductase enzymes localized to the cytosol and mitochondria, respectively (21, 25–27). Thus, by impairing ROS scavenging in high glucose TxNIP may contribute to "glucose toxicity." This has been observed in pancreatic β-cells as we and others have reported that TxNIP-deficient mice are relatively protected from the development of β-cell failure and diabetes induced by streptozotocin (28–30) and in the presence of insulin resistance (31). A similar role in promoting oxidative stress would implicate TxNIP in the pathogenesis of DN. To investigate this possibility and explore TxNIP action directly in the kidney, primary mesangial cells were cultured from wild-type control (C3H) and TxNIP-deficient (Hcb-19) mice and exposed to high glucose. TxNIP deficiency protected the mesangial cells (MC) from high glucose-induced increased ROS and collagen accumulation. Surprisingly, the lack of TxNIP was associated with a marked decrease in NADPH oxidase activity, ROS generation, and Nox4 induction rather than an increase in ROS scavenging. Furthermore, mitochondrial O_2^- was not increased by high glucose in Hcb-19 cells, whereas lactate production was augmented. These data place TxNIP upstream of NADPH oxidase activation by high glucose and suggest a potential Trx-independent action of TxNIP to promote mitochondrial metabolic flux, oxidative stress, and DN.

MATERIALS AND METHODS

Cell Culture—Mouse MC (passages 5–12) from C3H (wild-type TxNIP) and Hcb-19 (TxNIP- deficient) mice (kindly provided by R. Davis, University of California) were isolated and characterized as described (32, 33). They were propagated in Dulbecco's modified Eagle's medium (DMEM) supplemented with 10% FBS and 1% penicillin/streptomycin. At 70–80% confluence, cells were growth arrested with 0.5% FBS for 48 h and incubated with either 5.6 mM normal glucose (NG) or 25 mM high glucose (HG) for the times indicated. Cell lysates were obtained by homogenizing MCs in RIPA buffer containing Roche Complete protease inhibitors and passing them through a 26-gauge needle 10 times to disrupt the cells. The homogenates were centrifuged at 5000 × *g* for 10 min at 4 °C and supernatants were used immediately or stored at −80 °C.

Transfection of Small Interfering RNA (siRNA) and Recombinant Adenovirus—Stealth™ negative universal control and TxNIP-specific Stealth™ RNAi oligonucleotides (catalog number TXNIPMSS285710) were obtained from Invitrogen. Reverse transfections were performed using the reagents and protocols from INTERFERin™ Polyplus transfection. Briefly, control siRNA (50 nM) or TxNIP siRNA (50 nM) was mixed with polyplus reagent and serum-free Opti-MEM (Invitrogen) for 20 min at room temperature. Two hundred μl were added to the C3H MC containing 1.8 ml of DMEM (10% FBS) and then incubated for 24 h before growth arrest. The recombinant adenoviruses expressing green fluorescent protein (AdGFP) and TxNIP (Ad-TxNIP) were kindly provided by Dr. R. T. Lee (Harvard, Boston, MA). These viruses were amplified in 293A cells, purified, and concentrated using the Vivapure AdenoPACK100 kit (Cedarlane). Experiments were conducted using stock titer of 10^9 infectious units (ifu)/ml. Briefly, a mixture containing DMEM with 15% FBS, 2.5 mg/ml of poly-L-lysine and adenovirus was added to subconfluent Hcb-19 MC and incubated for 24 h before growth arrest. After preliminary dose-response experiments demonstrating levels of protein expression by immunoblotting (data not shown), 250 μl of stock in 1.75 ml of media (25×10^7 ifu/10^6 cells) to 1000 μl (10^9 ifu/10^6 cells) were chosen for these studies.

Western Blotting—Protein concentrations in total cell lysates were determined using the modified Lowry microassay (Bio-Rad). After boiling in 4× sample buffer, 20 μg of protein were separated by 10–15% SDS-PAGE, transferred onto nitrocellulose membranes, which were blocked with 5% milk/Tris-buffered saline with 0.1% Tween 20 as described (34), using the following specific primary and secondary antibodies. Primary antibodies (1:1,000) were TxNIP (MBL), Nox2 and rac1 (Millipore), MnSOD and Prohibitin (Abcam), Nox4 (Novus), GPx1 (Epitomics), HO-1, Catalase, and Trx1 (Cell Signaling) and all others from Santa Cruz Biotechnology (β-actin 1:10,000). Secondary antibodies (1:4,000) were anti-rabbit IgG HRP conjugate (Bio-Rad) and peroxidase-conjugated anti-mouse IgG (Jackson ImmunoResearch Labs). Immunoblots were visualized by the ECL detection system (KPL Mandel Scientific) and the densitometric analyses were performed using NIH ImageJ software.

Quantitative Real-time RT-PCR—RNA was extracted using the RNeasy Mini kit (Qiagen), reverse transcribed with an OmniScript RT kit (Qiagen) using random primers in a total volume of 20 μl according to the manufacturer's protocol. Real-time PCR using cDNA and SYBR Green PCR Master Mix (Applied Biosystems) was performed and analyzed on an ABI Prism 7900 HT Sequence Detection System (Applied Biosystem). The primers used were: Nox2 forward, 5′-TGATGTTAGTGGGAGCCGGGATTG-3′, Nox2 reverse, 5′-TCTGCAAACCACTCAAAGGCATG-3′; Nox4 forward, 5′-GGATCACAGAAGGTCCCTAGCAG-3′, Nox4 reverse, 5′-GCGGCTACATGCACACCTGAGAA-3′; and 18S forward, 5′-GGCTACCACATCCAAGGAA, 18S reverse, 5′-GCTGGAATTACCGCGGCT-3′. 18S RNA was used as the loading control. The relative amounts of mRNA were determined by $\Delta\Delta C_t$ calculations (35).

ROS and Mitochondrial Membrane Potential Measurement—MCs were cultured on glass coverslips and incubated in the dark with 1 μM carboxymethyl-H_2-dichlorofluorescein diacetate (CM-H_2DCFDA) or dihydroethidium (DHE) for 30 min at 37 °C. Intracellular ROS production was assessed with an Olympus FluoView 1000 Laser Scanning Confocal Microscope (excitation/emission at λ = 488 nm/515 nm for DCF; excitation/emission at 396 nm/579 nm for superoxide, and excitation/emission at 510 nm/580 nm for general ROS detection for DHE). Mitochondrial superoxide formation was detected by incubating cells in the dark with 5 μM MitoSOX Red dye (excitation/emission at λ = 510 nm/580 nm) for 30 min. To assess mitochondrial membrane potential, the cells were preincubated with 2 μl/ml of JC-1 dye (Invitrogen) for 30 min and detected at excitation/emission at λ = 590/610 nm for JC-1 aggregates and excitation/emission at λ = 485/535 nm for monomers. The average fluorescence intensity per cell for each experimental group of cells was calculated using NIH ImageJ analysis software. An average of 10 cells/field and at least 4–5 random fields/condition were chosen for each experiment and analyzed in a blinded manner. Hydrogen peroxide released by the cells was assessed by incubating the growth media (phenol red-free) from the cells in a reaction mixture containing Amplex Red (Invitrogen) and then determining the absorbance at 560 nm in a microplate reader, as per the manufacturer's instructions. The readings were then normalized by the number of cells for each condition.

The rate of hydrogen peroxide disappearance in MCs was assessed according to Chen *et al.* (40) with a slight modification. Briefly, growth-arrested cells were pretreated with 10 μM diphenyleneiodonium chloride (Sigma) for 1 h to inhibit endogenous NADPH oxidase and mitochondria-derived ROS (37). Then different concentrations of H_2O_2 (hydrogen peroxide) (1 μM-100 μM) were added to the cells and the changes in the levels of ROS were measured at various intervals using CM-H_2DCFDA dye and a Molecular Device plate reader at excitation/emission at λ = 485/538 nm. Based on the results from preliminary experiments, the rates of ROS decomposition were linear between 120 and 180 min post-H_2O_2 treatment; thus, the rates of ROS degradation under the various conditions were determined during this 1 h.

Mitochondria Isolation—MCs were harvested from the cultures and mitochondria were isolated using a ThermoFisher mitochondria isolation kit according to the manufacturer's instructions.

Confocal Imaging of Collagen α (Type IV)—MCs were cultured on glass coverslips and treated with NG or HG for 24 h after growth arrest. Cells were fixed in 3.7% formaldehyde, permeabilized in methanol, and blocked with 1% goat serum plus 0.1% BSA. Immunofluorescence staining was performed by incubating the fixed cells with collagen α (IV) primary antibody (1:250, Rockland) and FITC-conjugated secondary antibody (1:100, BD Transduction Labs) and viewed with an Olympus FluoView Confocal Microscope.

NADPH Oxidase Activity Assay—NADPH oxidase activity was measured using the lucigenin-enhanced chemiluminescence method as previously described (11). In brief, MCs were washed and homogenized in lysis buffer containing 20 mM KH_2PO_4 (pH 7.0), 1 mM EGTA and Complete protease inhibitors (Roche Applied Science). A total of 100 μl of homogenates were added to 900 μl of assay buffer comprising 50 mM KH_2PO_4 (pH 7.0), 1 mM EGTA, 150 mM sucrose, 5 μM lucigenin (electron acceptor), and 100 μM NADPH (electron donor). Photoemission was measured every 30 s for 5 min with a GloMax luminometer. A buffer without NADPH was used as blank. Rate of superoxide generation was calculated by subtracting the readings from the blank and expressed as relative light units per min per mg of protein.

Trx Activity Assay—After cell lysis, thioredoxin activity assay was performed according to Holmgren and co-workers (38), with modifications. Briefly, duplicate samples of 50 μg of protein (from cell lysates) were added to 40 μl of mixture 1 (400 μl of 1 M HEPES (pH 7.45), 160 μl of 0.2 M EDTA, 120 μl of NADPH (40 mg/ml), and 1000 μl of insulin (10 mg/ml)), bringing the final volume to 110 μl with water. To the first sample, 10 μl of Trx reductase was added, and to the second sample, 10 μl of water. The mixtures were incubated at 37 °C for 20 min and the enzymatic activity was stopped by adding 250 μl of stop buffer (6 M guanidine HCl and 0.4 mg/ml of 5,5′-dithiobis(nitrobenzoic acid)) to each tube. Two hundred μl from each tube was added to 96-well plates and readings were taken at 410 nm. The differences in the absorbance between Trx reductase and water-treated samples represent the thioredoxin activity in the cell lysates.

Lactate Concentrations—Lactate concentrations in the cell culture media were assessed using the Abcam Lactate Colorimetric Assay kit according to the manufacturer's instruction.

Statistical Analysis—Results are expressed as mean ± S.E. Statistical analysis was performed by analysis of variance followed by the Newman-Keuls method for multiple comparisons using GraphPad Prism 4. Comparison between two sets of samples was analyzed by Student's *t* test. $p < 0.05$ was considered to be statistically significant.

RESULTS

High Glucose Induces Expression of Collagen IV in Wild-type C3H but Not in TxNIP-deficient Hcb-19 Mesangial Cells—There is evidence in the literature demonstrating the effect of high glucose on the expression of TxNIP (39–41). In this study we verified that the primary mouse MCs harvested from C3H control mice exhibited a similar response. However, in Hcb-19 MC, which lack TxNIP protein due to a spontaneous nonsense mutation in the gene encoding TxNIP (42), showed no expression by immunoblotting (Fig. 1*A*). Thus, treatment with high glucose resulted in a time-dependent increase in TxNIP, which was significantly increased in wild-type C3H MC by 1 h of HG treatment, rising to ~15-fold by 24 h (Fig. 1*A*).

One of the hallmarks of DN is increased mesangial ECM protein deposition (2, 43). Therefore, we determined whether TxNIP was required for this outcome. Collagen α(IV), an ECM protein known to be associated with glomerulosclerosis was increased 1.7 ± 0.43-fold after a 24-h HG treatment of C3H MC, but no change was observed in Hcb-19 MC (Fig. 1*B*). These data, consistent with Kobayashi *et al.* (7), indicate that TxNIP is required for the induction of collagen IV protein by high glucose in MC.

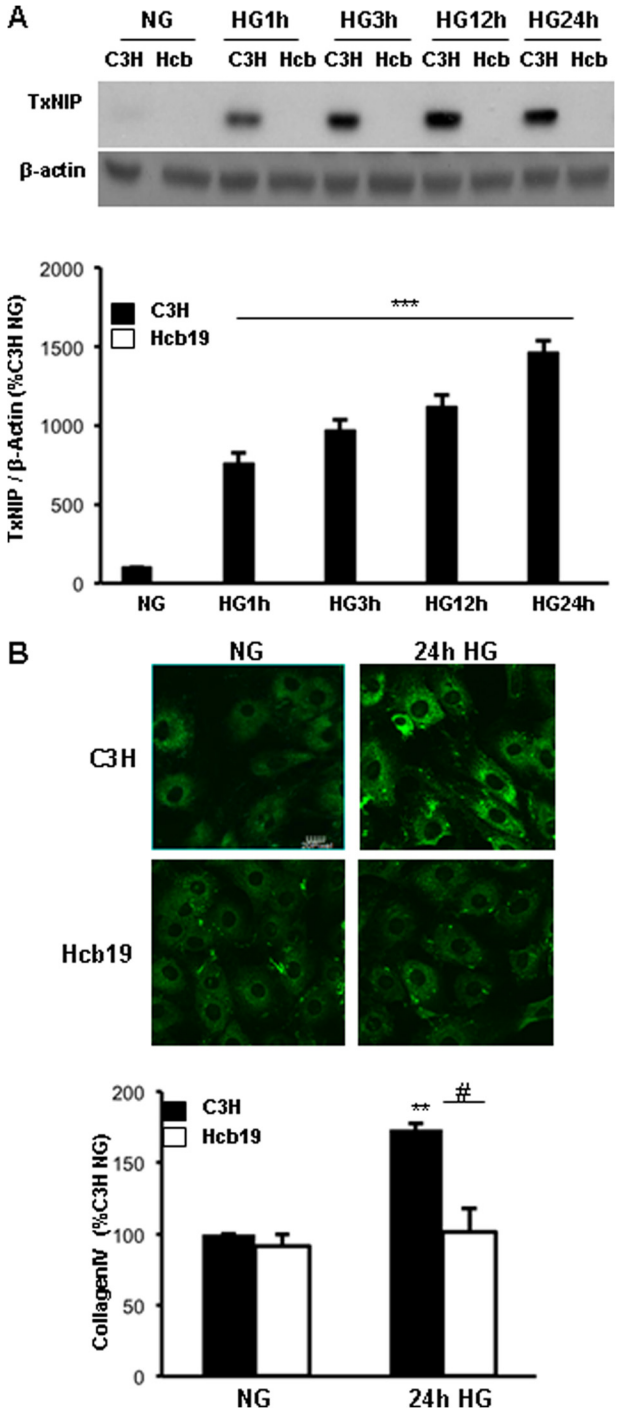

FIGURE 1. **HG-stimulated collagen accumulation is impaired in Hcb-19 TxNIP-deficient MC.** Growth-arrested MC (C3H, Hcb-19) were exposed to NG (5.6 mM) or HG (25 mM) for up to 24 h. *A,* proteins from total cell lysates were separated on SDS-PAGE and blotted for TxNIP and β-actin as loading control. *B*, collagen IV expression was analyzed by confocal microscopy and quantified by measuring pixel intensity per cell ($n = 150$ cells) in 3 independent experiments. Results (mean ± S.E.) are shown in the graphs. ***, $p < 0.0001$ *versus* C3H NG; **, $<p < 0.001$ *versus* C3H NG; and #, $p < 0.05$ *versus* C3H HG.

TxNIP Is Required for the High Glucose-induced Increase in MC ROS and Decrease in Trx Activity—Intracellular ROS production was assessed by preincubating mesangial cells with a cell-permeable fluorescent probe, CM-H_2DCFDA, which is oxidized to 2′7′-dichlorofluorescein by H_2O_2. As illustrated in Fig. 2*A*, HG-induced ROS production was augmented in C3H cells, peaking at 3 h of treatment. However, HG exposure did not increase ROS in the Hcb-19 cells. Similar experiments were performed using DHE, another biomarker for cellular ROS. Fluorescent detection of superoxide production by the MC (Fig. 2*B*) was assessed at excitation/emission at 396/579 nm, and total ROS (Fig. 2*C*) that forms ethidium at 510/580 nm, as described (44). The pattern of superoxide and total ROS generation were similar to the results obtained from the DCF experiments (Fig. 2, *B* and *C*). To confirm that ROS signaling in C3H and Hcb19 cells (Fig. 2, *A–C*) were not due to differences in the uptake of the dye by the different cells, the amount of H_2O_2 released was also assessed by the levels of resorufin (red fluorescent-oxidized product of Amplex Red reagent) in the cell culture media. As seen in Fig. 2*D*, the amount of H_2O_2 generated by the cells was similar to the ROS detected by DCF/DHE (Fig. 2, *A–C*). Together, these data indicate that without TxNIP, there appears to be either an impairment in ROS generation or an increase in endogenous ROS scavenging/antioxidant capacity.

To gain insight into the extent of Trx activity available to scavenge intracellular ROS, a Trx activity assay was performed using a modified version of the protocol of Holmgren and coworkers (38). Interestingly, there was a significant reduction in the Trx activity in C3H MC by 1 h of HG treatment that was decreased by 69% (*versus* C3H NG) at 3 h post-treatment (Fig. 2*E*). This decline in Trx activity, representing oxidation/inactivation of endogenous Trx by the ROS and/or inhibition by TxNIP, could have partially accounted for the observed increase in ROS (Fig. 2, *A–D*). On the other hand, although there was a trend toward a decrease in Trx activity in high glucose in Hcb-19 cells, the difference was not statistically significant.

H_2O_2 Scavenging Is Not Augmented in TxNIP-deficient Mesangial Cells—The lack of a significant decrease in endogenous Trx activity in TxNIP-deficient cells in the presence of high glucose was surprising and suggested that either there existed such an excess of antioxidant activity that a decrease was not detected, or that ROS generation was impaired. To more directly determine the ability of Hcb-19 MC to dissipate ROS, cells were exposed to 1 and 10 μM H_2O_2 and ROS disappearance was monitored over time by DCF fluorescence as described under "Materials and Methods." The rate of disappearance of ROS was lower in Hcb-19 compared with C3H MC (Fig. 2*F*). These results appeared paradoxical because TxNIP is known to inhibit Trx and thus antioxidant activity. However, whereas Trx1 and -2 protein levels were minimally decreased in the basal state in Hcb-19 cells, they were rapidly up-regulated (3 h) in high glucose in C3H but not altered in Hcb-19 MC (Fig. 3). Together, these data suggested a defect in ROS generation in Hcb-19 cells.

High Glucose-stimulated NADPH Oxidase Activity and Nox4 Expression Are Impaired in Hcb-19 Cells—A significant source of high glucose-stimulated ROS is NADPH oxidase. To investigate its role in the decreased ROS generation in TxNIP deficiency, NADPH oxidase activity was measured before and after various times of high glucose exposure. Superoxide generation by the NADPH oxidase system was assessed by the lucigenin-enhanced chemiluminescence method in total cell lysates from MC treated with HG for 3 and 24 h. NADPH oxidase activity was decreased in the basal state in the absence of TxNIP in Hcb-19 MC (Fig. 4*A*). After 3 h of HG exposure there was a

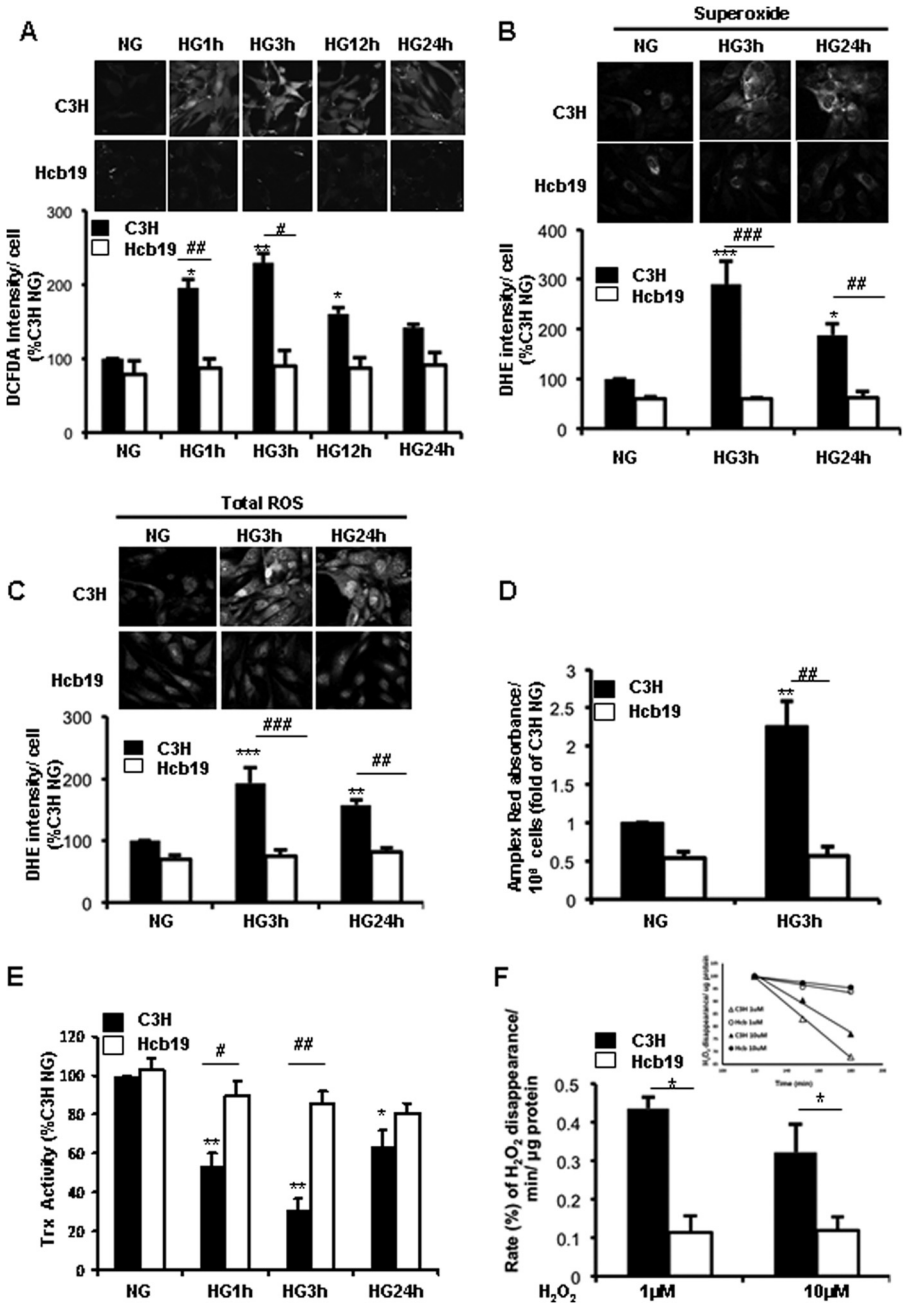

FIGURE 2. **High glucose-induced ROS and concomitant decrease in Trx activity is impaired in TxNIP-deficient Hcb-19 MC.** MCs were exposed to NG (5.6 mM) or HG (25 mM) for up to 24 h. *A-C*, MC were assessed by confocal microscopy after DCF or DHE treatments for 30 min. The images were quantified as pixel intensity and expressed as % of C3H NG designated as 100 ($n = 3$ independent experiments). *D*, H_2O_2 released by the cells was measured in 50 μl of cell culture media preincubated with Amplex Red reagent for 30 min ($n = 6$; results were normalized for the number of cells). *E*, after cell lysis, Trx activity ($n = 5$) was performed as described under "Materials and Methods." Results are expressed as mean ± S.E. *, $p < 0.01$ *versus* C3H NG; **, $p < 0.001$ *versus* C3H NG; #, $p < 0.05$ *versus* C3H 1-h HG; ##, $p < 0.001$ *versus* C3H 3- or 24-h HG; and ###, $p < 0.0001$ *versus* C3H 3-h HG. *F*, C3H and Hcb-19 MC were pretreated with 10 μM diphenyleneiodonium chloride for 1 h and then exposed to 1 and 10 μM H_2O_2 for a total of 4 h. The decline in ROS was assessed between 2 and 3 h post-treatment (see *inset* for slopes) by DCF fluorescence microscopy and the relative (%) decreases in fluorescence intensities expressed as the rate of disappearance/min. Results are mean ± S.E. from 4 independent experiments. *, $p < 0.05$ *versus* C3H at 1 or 10 μM concentrations.

2.3 ± 0.16-fold increase in superoxide production in C3H MC that remained higher at 24 h. In contrast, there were no significant changes in superoxide production in Hcb-19 cells after 3 or 24 h of HG (Fig. 4*A*). The two major isoforms of NADPH oxidase, which are expressed in kidney, are Nox2 and Nox4 with a small amount of Nox1 (4, 45). Indeed, Nox4, also known as "renox," is the most highly expressed. To investigate the contribution of Nox isoforms in the HG-induced NADPH oxidase activity, we determined their levels in the two cell types. Nox1 was only weakly detected, showed no difference between C3H and Hcb-19 MC, and was not up-regulated by HG (Fig. 5*A*). Nox2 was readily detected but also not different. We observed a trend toward increased Nox2 in HG in C3H MC but this did not reach statistical significance even after 24 h (Fig. 4*B*). In addition, *Nox2* mRNA was not altered by HG in either C3H or Hcb-19 MC (Fig. 4*D*). In contrast, Nox4 protein was lower in

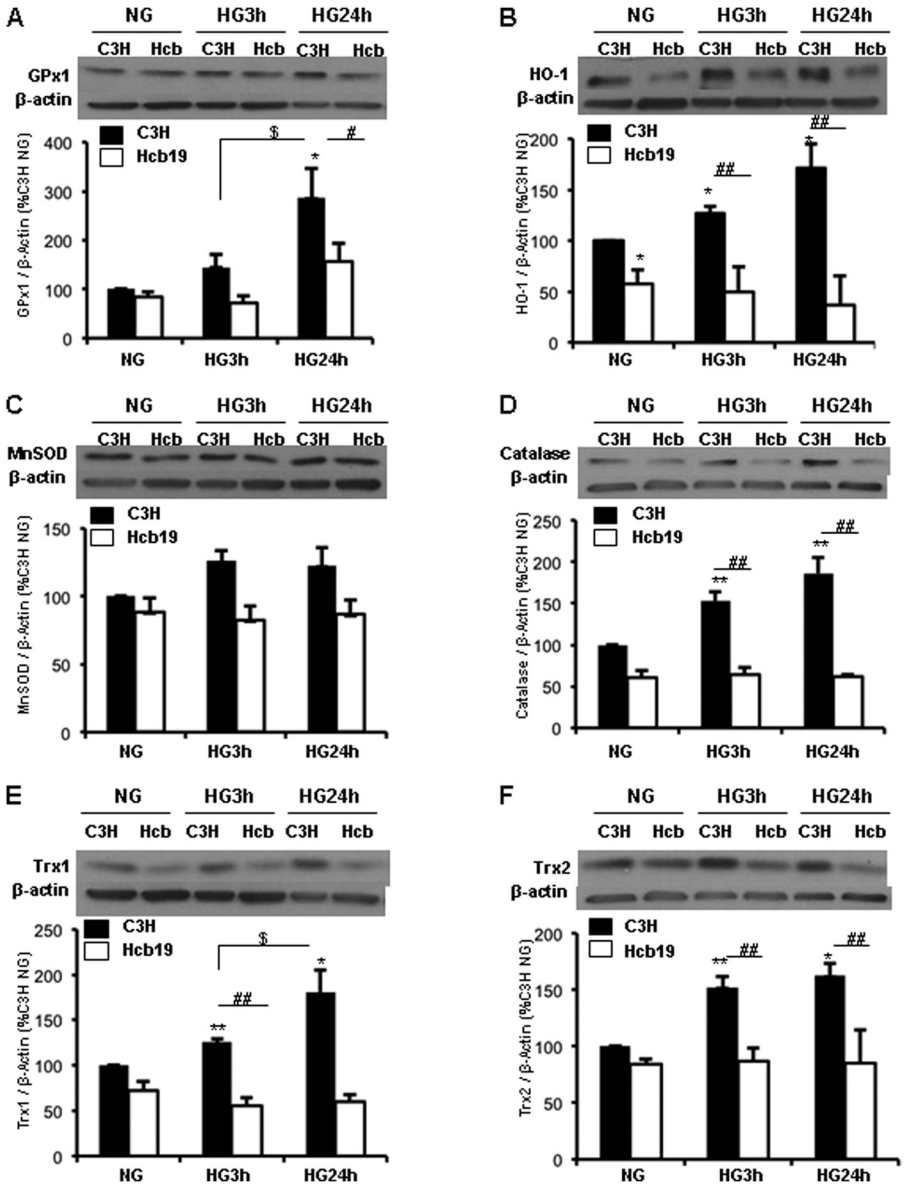

FIGURE 3. **HG effects on endogenous antioxidants in C3H and Hcb-19 (TxNIP-deficient) MC.** C3H and Hcb-19 MC were cultured in NG (5.6 mM) or HG (25 mM) for 3 and 24 h. Immunoblotting was performed on total cell lysates for: *A,* GPx1; *B,* HO-1; *C,* MnSOD; *D,* catalase; *E,* Trx1; and *F,* Trx2, whereas β-actin served as loading control. The results were normalized to C3H NG, and depicted in the graphs *below* the respective images. Results are mean ± S.E. ($n = 4$). *, $p < 0.05$ *versus* C3H NG; **, $p < 0.001$ *versus* C3H NG; $, $p < 0.05$ *versus* C3H 3-h HG; #, $p < 0.01$ *versus* C3H 24-h HG; and ##, $p < 0.001$ *versus* C3H 3- and 24-h HG.

TxNIP-deficient Hcb-19 MC in the basal state and not altered by HG, whereas in C3H Nox4 was rapidly induced (3 h) and remained elevated at 24 h (Fig. 4*C*). Similar results were obtained by real-time RT-PCR assessment of *Nox4* mRNA, which was increased by HG only in C3H MC (Fig. 4*E*). The increase in NADPH oxidase activity stimulated by HG has also been associated with up-regulation of other Nox-associated subunits such as $p47^{phox}$, $p67^{phox}$, rac1, and $p22^{phox}$ (4, 13, 15, 46, 47). Although $p22^{phox}$ could contribute to Nox2 and/or Nox4, the former 3 proteins are associated with Nox2 activity (4, 45, 48, 49). Under these conditions there was a significant but transient increase in $p47^{phox}$ induced by HG in C3H, which returned to basal levels after 24 h. However, there was no change detected in Hcb-19 (Fig. 5*B*). Similarly, there were no changes caused by HG in $p67^{phox}$ or rac1 in either cell type (Fig. 5, *C* and *D*). $p22^{phox}$ was also significantly induced by HG only in C3H MC, and this increase was maintained at 24 h (Fig. 5*E*). Thus, whereas we cannot rule out a contribution to the HG-stimulated NADPH oxidase activity of Nox2 at 3 h, these data suggest that Nox4 is the major isoform involved, particularly at 24 h. In addition, TxNIP is necessary for up-regulation of Nox4 as well as the subunits, $p47^{phox}$ and $p22^{phox}$ in HG.

High Glucose Promotes ROS Production and Nox4 Protein Expression in the Mitochondria of C3H MC—There are studies that have demonstrated that Nox4 siRNA or antisense oligonucleotides block high glucose-induced increases in mesangial cell ROS, *i.e.* cytosolic NADPH oxidase activity as well as mitochondrial superoxide formation, indicating that Nox4 is essential for HG-induced MC ROS generation (14, 16). These findings are also consistent with the observation that Nox4 is an important mediator of mesangial matrix accumulation in diabetes (14).

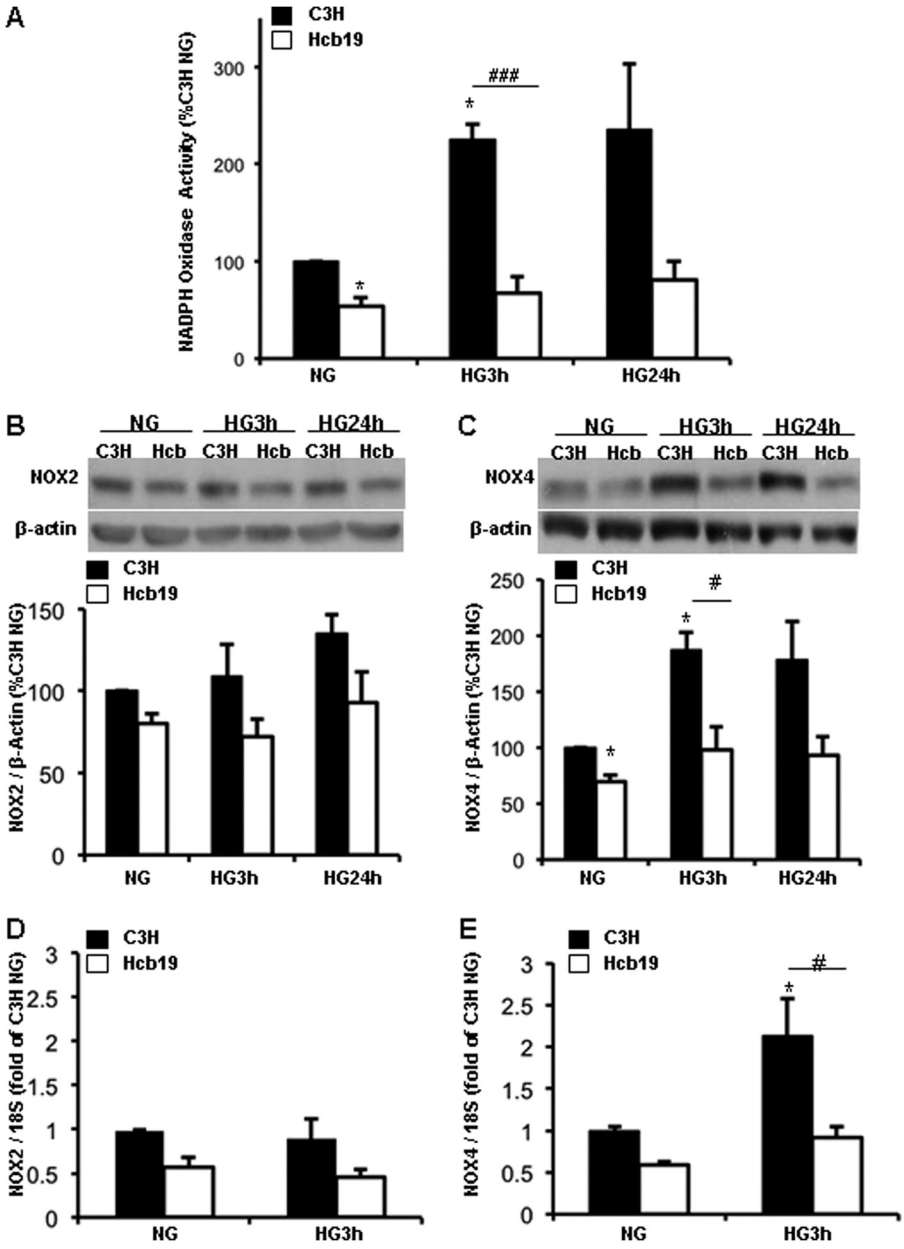

FIGURE 4. **High glucose augments NADPH oxidase activity and Nox4 expression in C3H but not in Hcb-19 MC.** *A*, NADPH oxidase activity in the total cell lysates isolated from NG (5.6 mM) or HG (25 mM)-treated MC was measured as NADPH-dependent superoxide generation with the lucigenin-enhanced chemiluminescence method ($n = 4$). *B* and *C*, expression of Nox2 and Nox4 protein in total cell lysates was assessed by immunoblotting ($n = 4$). *D* and *E*, *Nox2* and *Nox4* mRNA expression was assessed by real-time PCR ($n = 6–7$). Values are mean ± S.E. *, $p < 0.01$ *versus* C3H NG; #, $p < 0.05$ *versus* C3H 3-h HG; and ###, $p < 0.0001$ *versus* C3H 3-h HG.

To examine mitochondria-specific ROS generation and Nox4 expression, MC were treated with HG for varying times and superoxide generation in live cells was measured with MitoSOX Red, a mitochondria-specific fluorogenic dye that produces red fluorescence upon being oxidized by superoxide. By 1 h of HG treatment, there was a significant rise in mitochondrial superoxide production in C3H MC, which remained elevated up to 24 h of HG treatment (Fig. 6*A*). However, mitochondrial ROS production by Hcb-19 MC was not affected by HG (Fig. 6*A*), indicating mitochondrial dysfunction, at least in this respect, in Hcb-19 cells lacking TxNIP.

In MC, Nox4 has been found to primarily localize to mitochondria and to a lesser extent to plasma membranes (16). Thus, the expression of Nox4 in mitochondrial extracts from HG-treated MCs was examined. The mitochondrial fractions were prepared as described under "Materials and Methods" and purity was verified by immunoblotting of the mitochondrial markers prohibitin, COX IV and VDAC/porin (Fig. 6*B*). As shown in Fig. 6*C*, there was a dramatic increase in Nox4 levels in HG-treated C3H cells, but in Hcb-19, mitochondrial Nox4 expression remained unaffected. Therefore, it appears that TxNIP plays an important role in inducing mitochondrial Nox4, which in turn contributes to the ROS production.

Knockdown of TxNIP in Wild-type C3H MC Mimics the Features of Hcb-19 Cells—To verify that the defects in ROS generation, NADPH oxidase activation and Nox4 expression upon

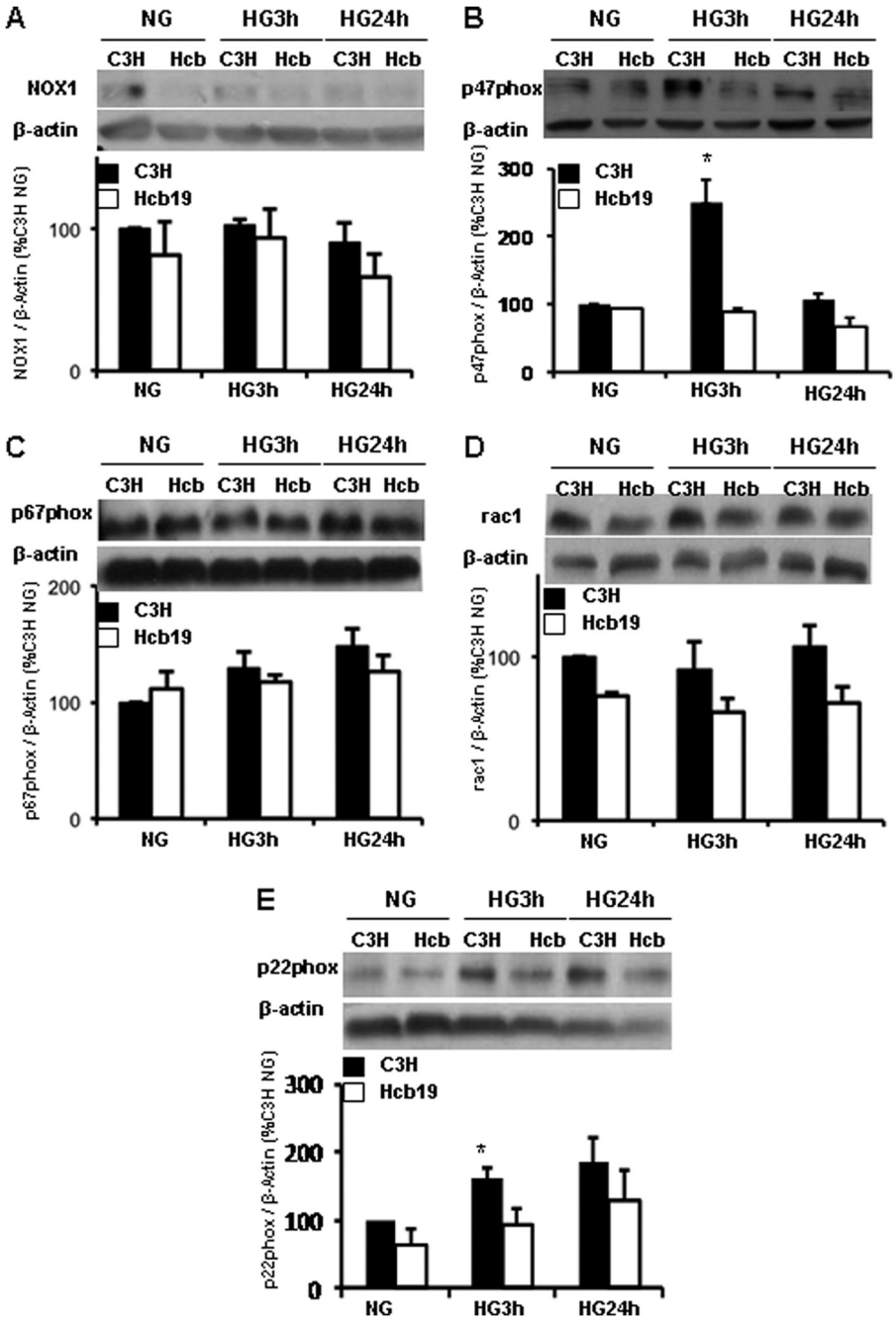

FIGURE 5. **Effect of HG on isoforms and subunits of NADPH oxidase in MC.** Growth-arrested MC from C3H and Hcb-19 mice were cultured in NG (5.6 mM) or HG (25 mM) for 3 and 24 h. Total cell lysates were subjected to immunoblotting for: *A*, Nox1; *B*, p47^{phox}; *C*, p67^{phox}; *D*, rac1; and *E*, p22^{phox}, with β-actin as loading control. The results were normalized to C3H NG, and are represented in graphs below the respective images. Results are mean ± S.E. (n = 3–4 independent experiments). *, $p < 0.05$ *versus* control C3H NG; #, $p < 0.05$ *versus* C3H 3-h HG.

HG exposure in TxNIP-deficient Hcb-19 MC were caused by the lack of TxNIP, the wild-type C3H cells were treated with TxNIP-specific or scrambled siRNA. TxNIP protein was effectively decreased upon knockdown with siRNA in HG to levels even below that of scrambled siRNA-transfected cells and completely blocked the up-regulation of TxNIP by HG (Fig. 7*D*). This decrease in TxNIP markedly inhibited HG-stimulated cellular ROS monitored by DCF fluorescence (Fig. 7*A*), mitochondria-specific ROS detected with MitoSox (Fig. 7*B*), and NADPH oxidase activity (Fig. 7*C*). In addition, TxNIP knockdown blocked Nox4 induction (Fig. 7*D*) in response to HG and collagen IV accumulation, an *in vitro* marker of the increased ECM protein in DN (Fig. 7*E*). These results in C3H cells with TxNIP-specific knockdown indicate the requirement of TxNIP as a mediator of HG signaling.

Overexpression of TxNIP in Hcb-19 MC Augments Mitochondrial ROS and Nox4—To confirm the functional role of TxNIP in HG signaling, the TxNIP-deficient Hcb-19 MC were transduced with TxNIP expressing adenovirus (AdTxNIP) or control GFP expressing adenovirus (AdGFP). Dose-response experiments revealed that 25×10^7 ifu/ml/well (10^6 cells) for 24 h resulted in TxNIP protein levels that were at least as high as

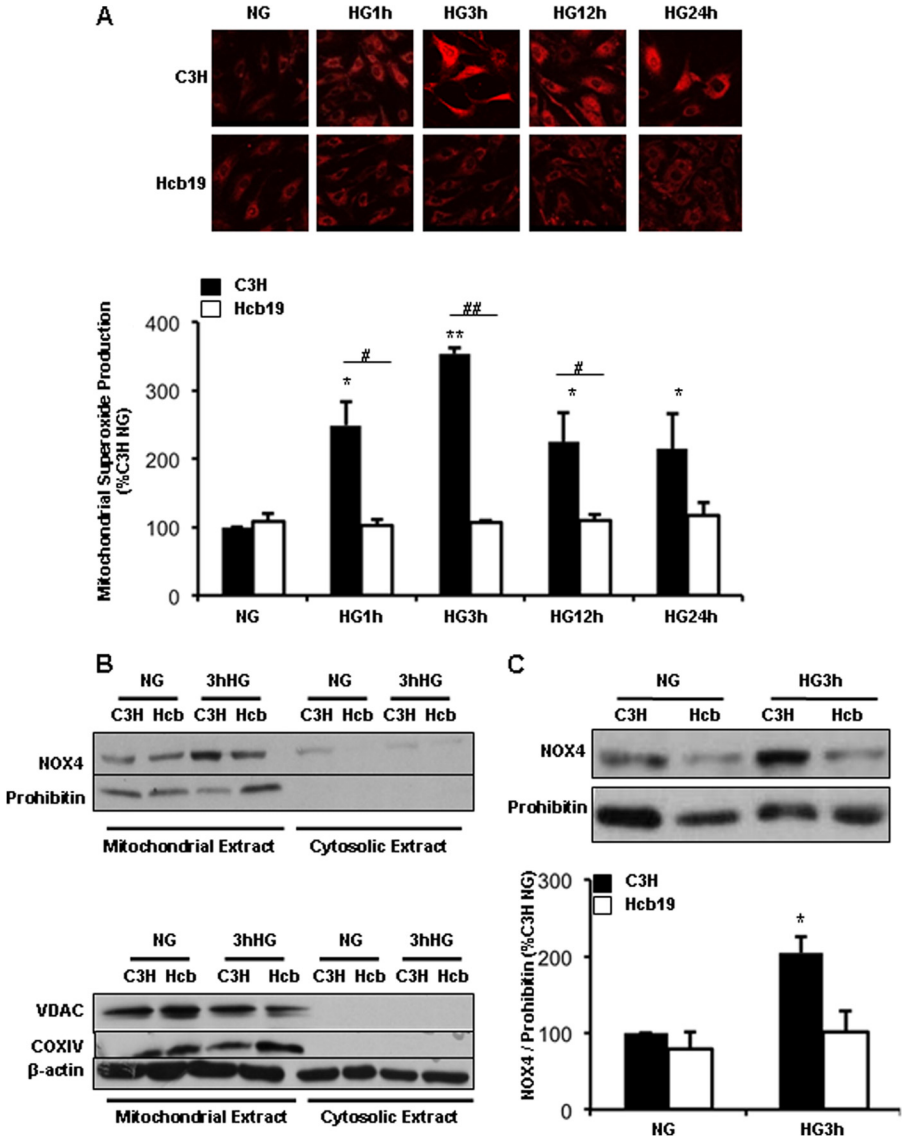

FIGURE 6. **Mitochondrial ROS and Nox4 protein expression in MC requires TxNIP.** C3H and Hcb-19 MC were treated with NG (5.6 mM) or HG (25 mM) for the times indicated. *A*, ROS levels were determined by confocal microscopy after MitoSOX treatment for 30 min. The images were analyzed using ImageJ software and normalized to C3H NG designated as 100%. *B*, mitochondrial and cytosolic extracts were obtained from the total cell lysates and immunoblotted for the mitochondrial markers, prohibitin, VDAC, and COX IV as described under "Materials and Methods." *C*, mitochondrial expression of Nox4 and prohibitin (mitochondrial loading control) were assessed by immunoblotting. Results are mean ± S.E. ($n = 3$). *, $p < 0.05$ *versus* control C3H NG; **, $p < 0.001$ *versus* C3H NG; ##, $p < 0.05$ *versus* C3H HG; and ##, $p < 0.001$ *versus* C3H HG.

those observed after HG exposure of C3H MC (Figs. 1*A* and 8*B*). Mitochondrial O_2^- production was then examined in normal and HG. As expected, HG stimulated mitochondrial O_2^- in control AdGFP-transfected C3H MC (1.96 ± 0.22-fold of NG, $p < 0.05$) but not in AdGFP Hcb-19 (Fig. 8*A*). However, AdTxNIP-transfected Hcb-19 cells showed increased MitoSox fluorescence in normal glucose (~2-fold of AdGFP Hcb-19), which did not increase further with HG treatment (Fig. 8*A*). Measurement of Nox4 protein showed a TxNIP dose-dependent increase in Hcb-19 cells in normal glucose, which also did not increase further in HG (Fig. 8*B*). These data indicate that TxNIP, when expressed at levels similar to that observed with HG in MC, induces mitochondrial ROS and Nox4 expression and support the notion that it plays a key role in diabetic nephropathy.

TxNIP Is Required for the High Glucose-associated Increase in Mitochondrial/TCA cycle Glucose Metabolism—TxNIP has been recently implicated as a "gatekeeper" of pyruvate conversion to acetyl-CoA for mitochondrial glucose oxidation via the TCA cycle and electron transport (50). Cardiomyocytes from $TxNIP^{-/-}$ mice display increased glycolysis and lactate production, a Warburg-like effect (50). Evidence for this metabolic pattern was observed in Hcb-19 MC in which exposure to HG resulted in a significant elevation of lactate concentrations in the medium that was not observed in C3H (Fig. 9*A*).

Glucose metabolite flux and oxidation in mitochondria were assessed by measuring the mitochondrial membrane potential. Mitochondrial membrane potential is increased by flux through the electron transport chain and generation of a proton gradient across the membrane (51). JC-1 is a cationic dye that

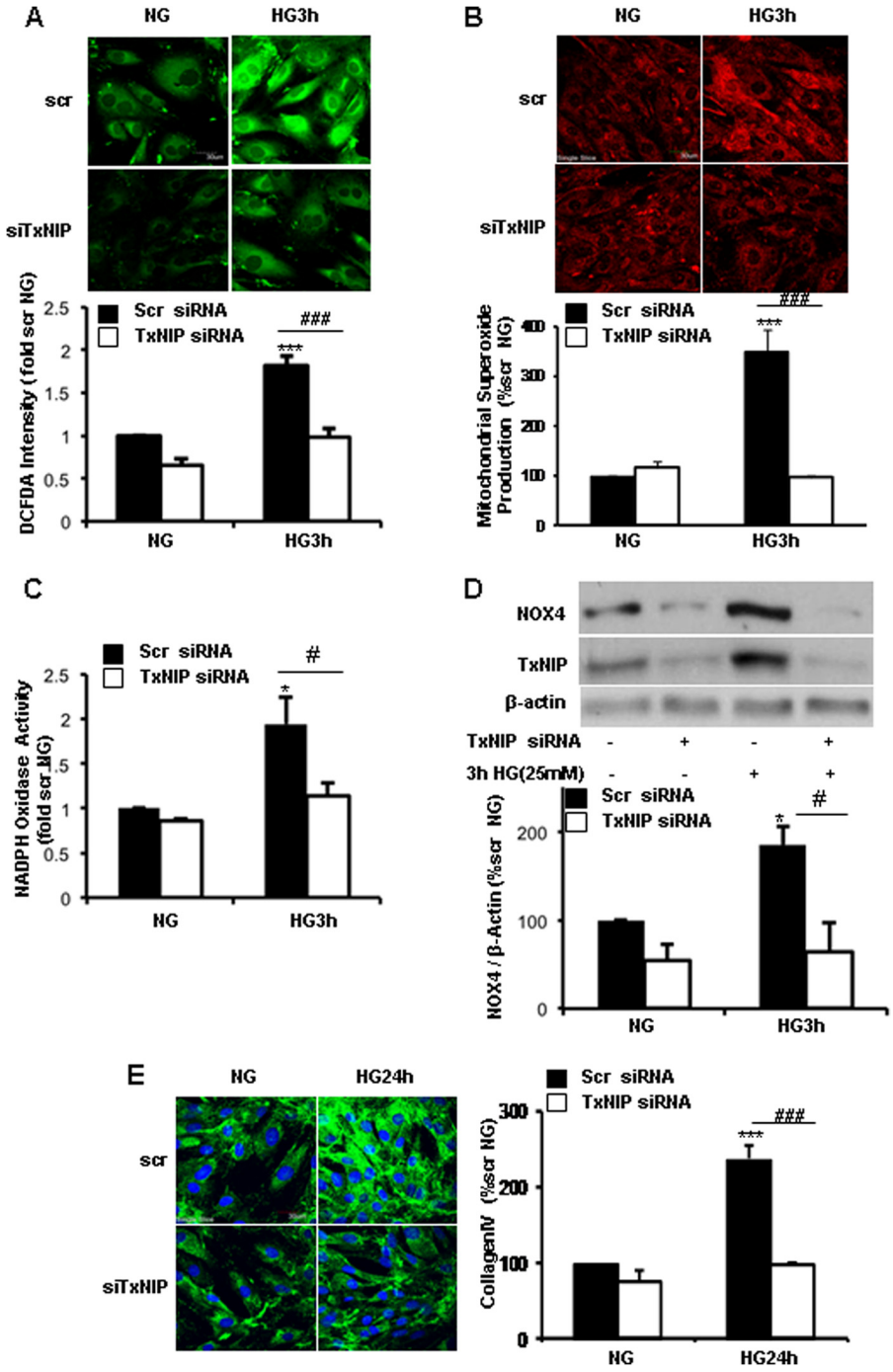

FIGURE 7. **TxNIP knockdown in C3H MC mimics the defects in response to HG observed in Hcb-19 MC.** C3H MC were transfected with 50 nM TxNIP-specific siRNA (*siTxNIP*) or universal negative control siRNA (scrambled, *scr*) for 24 h and then incubated in NG (5.6 mM) or HG (25 mM) for 3 or 24 h. *A* and *B*, intracellular ROS and mitochondrial superoxide formation were assessed by confocal microscopy using DCF and MitoSOX, respectively ($n = 3$). *D*, Nox4 expression was measured in total cell lysates of the transfected cells by immunoblotting. Values are mean ± S.E. ($n = 3$). *, $p < 0.05$ *versus* scr siRNA NG; ***, $p < 0.001$ *versus* scr siRNA; #, $p < 0.05$ *versus* scr HG; and ###, $p < 0.001$ *versus* scr HG. *E*, collagen IV expression was analyzed by confocal microscopy and quantified by measuring pixel intensity per cell (150 cells) in 3 independent experiments. Results are mean ± S.E. ($n = 3$) depicted in the graphs. *C*, NADPH oxidase activity in the total cell lysates isolated from NG (5.6 mM) or HG (25 mM)- treated MC, transfected with scrambled siRNA or siTxNIP, was measured as NADPH-dependent superoxide generation with the lucigenin-enhanced chemiluminescence method ($n = 4$).

selectively enters and accumulates in mitochondrial matrix, where it forms J-aggregates with intense red fluorescence upon exceeding critical concentrations, thereby changing its color from green to red as the membrane potential is increased (52). In control C3H MC, mitochondrial membrane potential increased when HG was added forming red JC-1 aggregates (Fig. 9*B*, *upper panel*). In contrast, in Hcb-19 cells, JC-1 remained in its monomeric form as shown by green fluorescence (Fig. 9*B*, *lower panel*), indicating that mitochondrial glucose metabolism was not augmented in these cells. These results support the concept that TxNIP plays a key role augmenting glucose metabolic flux via the TCA cycle and that the defects in HG signaling may be mediated, at least in part, by this deficiency in mitochondrial function.

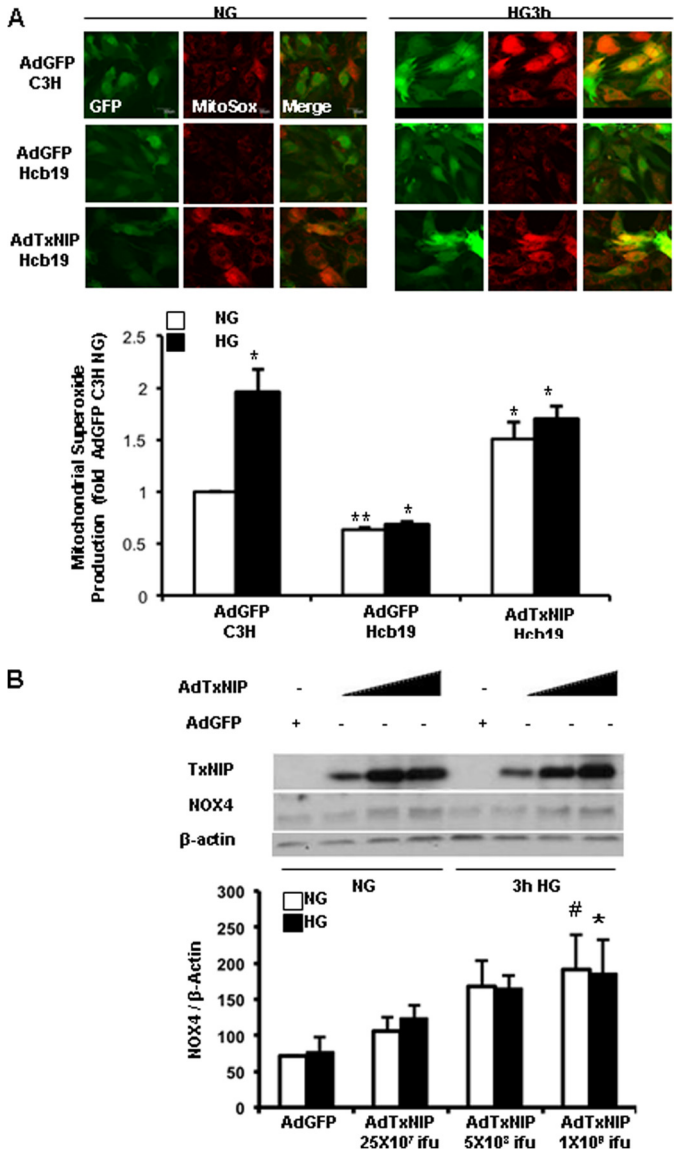

FIGURE 8. **Overexpression of TxNIP in Hcb-19 MC restores mitochondrial ROS and Nox4 expression.** Hcb-19 cells were transduced with GFP (*AdGFP*) or TxNIP (*AdTxNIP*) adenoviruses and C3H cells with AdGFP alone to serve as a control. After 24 h, cells were growth arrested for 48 h and then exposed to NG (5.6 mM) or HG (25 mM) for 3 h. *A,* mitochondrial superoxide production in the MC was determined with MitoSOX dye by confocal microscopy. Quantification is illustrated in the graph. Results are mean ± S.E. *, $p < 0.05$; and **, $p < 0.001$ *versus* AdGFP C3H NG. *B,* immunoblotting for Nox4 and TxNIP was performed using lysates from Hcb19 MC transduced with varying concentrations of AdTXNIP (25×10^7, 5×10^8, and 1×10^9 ifu/ml) in NG or HG. Results are mean ± S.E. ($n = 4$). *, $p < 0.05$ *versus* AdGFP Hcb19 NG.

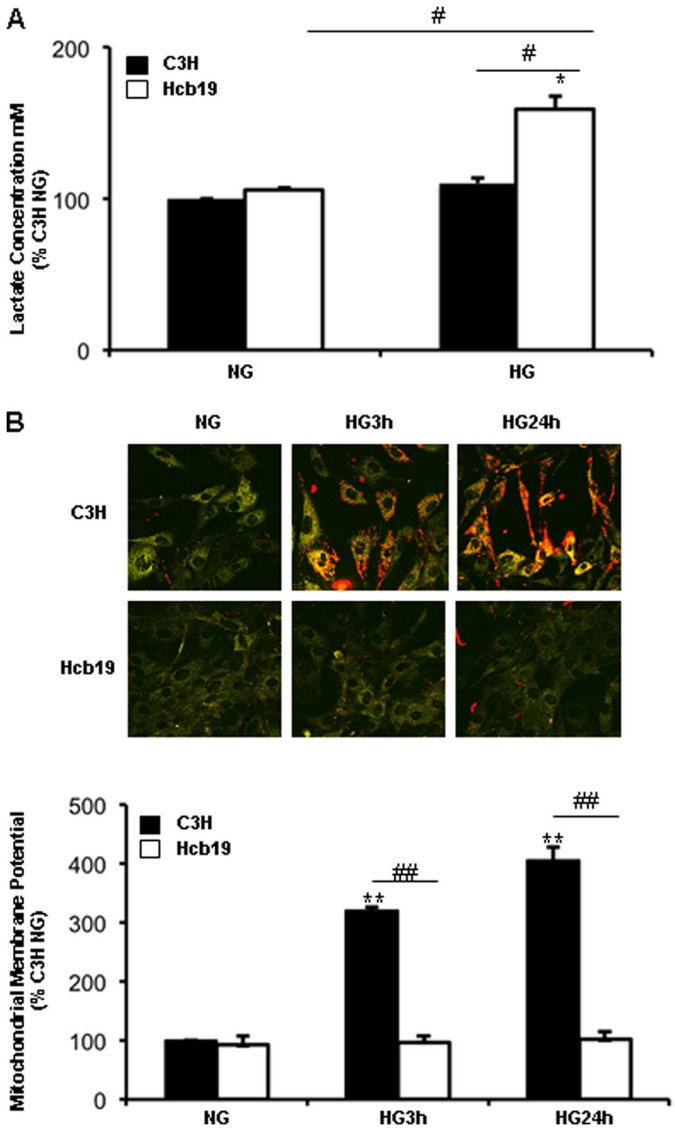

FIGURE 9. **TxNIP-deficient Hcb-19 MC show impaired mitochondrial glucose metabolism and increased lactate production.** Growth arrested MC (C3H, Hcb-19) were exposed to NG (5.6 mM) or HG (25 mM) for up to 24 h. *A,* lactate concentrations in the cell culture media. Results are mean ± S.E. ($n = 4$), *, $p < 0.05$ *versus* C3H NG; and #, $p < 0.05$ *versus* Hcb-19 HG. *B,* MC fluorescence was observed by confocal microscopy after JC-1 treatment for 30 min. The images were analyzed using ImageJ software and normalized to C3H NG. Quantification is illustrated in the graph. Results are mean ± S.E. ($n = 3$). **, $p < 0.001$ *versus* C3H NG; and ##, $p < 0.001$ *versus* C3H 3- and 24-h HG.

DISCUSSION

The importance of elevated levels of ROS in the pathogenesis of the microvascular complications of diabetes has been well documented (11, 12, 53). Although increased mitochondrial glucose oxidation and flux through the electron transport chain have been suggested to be the primary source, elevated NADPH oxidase activity has also been demonstrated to contribute to increased ROS and ultimately, to profibrotic signaling in the kidney stimulated by hyperglycemia (11–15). The cellular levels of ROS and the presence of oxidative stress are determined not only by rates of ROS generation, but also their neutralization and degradation by endogenous antioxidants. It has been proposed that by binding to and inhibiting the antioxidant Trxs, TxNIP up-regulation by HG promotes oxidative stress (27, 54). A specific role in the kidney was suggested by Kobayashi *et al.* (7) who showed that overexpression of TxNIP in cultured MC led to increased collagen IV mRNA and protein. A truncated TxNIP mutant that failed to bind Trx lacked this effect (7). In this study, we found a rapid, marked and sustained up-regulation of TxNIP in primary cultures of wild-type C3H MC exposed to HG. This was associated with increased production of ROS and collagen accumulation. In contrast, in Hcb-19 TxNIP-deficient MC, exposure to HG did not stimulate ROS or increase collagen. We reasoned that the inhibition of Trx in HG by augmented TxNIP would limit the dissipation of ROS and promote oxidative stress and that an absence of TxNIP would

permit a more effective antioxidant neutralizing capacity. However, in the Hcb-19 MC the TxNIP deficiency was associated with a lack of response to HG of NADPH oxidase activity and up-regulation of the major renal NADPH oxidase isoform, Nox4. These data indicated a defect in ROS generation. Indeed, direct assessment of H_2O_2 dissipation in the two MC lines revealed that in contrast to what was expected, ROS degradation was decreased in the absence of TxNIP. In the Hcb-19 MC, the protein content of several endogenous antioxidant enzymes including Trx1, Trx2, catalase, and HO-1 (hemoxygenase-1) tended to be lower in the basal state and showed no increase in HG in contrast to C3H MC (Fig. 3). Although we cannot rule out a contribution of Nox2 to the HG-induced NADPH oxidase activity in C3H MC, the lack of up-regulation of $p47^{phox}$ and $p22^{phox}$ in Hcb-19 MC (Fig. 5) would also be consistent with an absent NADPH oxidase response to HG without TxNIP.

The mechanism of up-regulation of Nox4 by HG is not clear. However, there are multiple stimulatory transcriptional regulators including NFκB, HIF1-α, AP-1, and Nrf-2 (55–59), which may all be activated by HG (10, 11, 60). Under basal conditions, Trx in mitochondria binds and inhibits ASK (apoptosis signal-regulating kinase)-1, an upstream MKK3/6 and p38 MAPK activator (61–63). TxNIP up-regulation has been proposed to bind Trx and release ASK-1 to activate p38 (64–66), which in turn would stimulate AP-1 (67, 68). In support of this possibility, TxNIP has recently been reported to translocate to the mitochondria in the presence of ROS in pancreatic β-cells (65). It has also been found that NFκB transcriptional activation requires ROS (69) and NFκB is activated in response to HG in endothelial cells (70). Recently, the activation of Nrf-2 in response to the increased ROS induced by HG has been documented and appears to be a negative feedback, protective pathway by inducing an antioxidant response (71). The lack of up-regulation of enzymes such as *HO-1*, a Nrf-2 responsive gene, in Hcb-19 MC in HG is consistent with the absence of ROS generation.

Because ROS are well documented cell signaling molecules, it is not clear whether the defect(s) observed in NADPH oxidase activation is primary or secondary. In this context, we examined mitochondria-specific ROS generation using MitoSox. In contrast to controls, in the absence of TxNIP, there was no increase in mitochondrial ROS (O_2^-) in response to HG in Hcb-19 MC. The key role of TxNIP was demonstrated by reproducing these defects in wild-type C3H MC using TxNIP-specific siRNA-mediated knockdown (Fig. 7). Thus, decreased total cellular ROS and mitochondrial O_2^- was associated with decreased NADPH oxidase activity, Nox4, and collagen expression, were documented in response to HG in C3H MC with TxNIP knockdown compared with C3H MC transfected with scrambled siRNA. Furthermore, restoration of TxNIP by adenoviral expression induced mitochondrial ROS and Nox4 expression in Hcb-19 cells even in the absence of HG.

Increased mitochondria-derived ROS in response to HG has been proposed to act as an initiator of the alterations in glucose metabolic pathways that contribute to the complications of diabetes (9–11). Thus, a relevant action of TxNIP could be its recently appreciated function to regulate glucose metabolism, specifically to increase mitochondrial glucose oxidation (50). In cardiomyocytes, protection from ischemia-reperfusion injury in intact hearts from $TxNIP^{-/-}$ mice was associated with increased glycolysis to lactate and a defect in entry of pyruvate into the Krebs cycle (50). In HG, increased mitochondrial glucose oxidation is observed and we found a marked increase in the mitochondrial membrane potential in C3H MC exposed to HG. However, this increase was completely absent in TxNIP-deficient Hcb-19 MC (Fig. 9) and was accompanied by an increase in lactate. These data in MC are similar to the glucose metabolic phenotype reported in cardiomyocytes and are consistent with a primary mitochondrial defect in ROS generation. It is not clear whether this metabolic effect is mediated by the Trx binding site of TxNIP or possibly, by its α-arrestin domain (72).

In summary, this study demonstrates widespread defects in ROS generation in response to HG in MC, which lack TxNIP, from both mitochondria and NADPH oxidase(s). Although TxNIP inhibits the endogenous antioxidant Trx, the decrease in ROS is not due to more rapid degradation of these reactive molecules, but appears to be mediated, at least in part, by a defect in regulating glucose metabolic flux to the TCA cycle. Although we cannot exclude other direct actions of TxNIP, which binds various proteins (73–75), this defect in mitochondrial and Nox4-mediated ROS generation would inhibit multiple signaling pathways such as PKC, advanced glycation end product formation, *O*-glycosylation, and TGF-β1, activated by high glucose. Thus, the lack of TxNIP was associated with protection from the pro-fibrotic signaling to collagen expression by HG. In view of the marked up-regulation of TxNIP and the key signaling role of ROS in HG-induced microvascular complications, TxNIP may be a relevant and powerful novel therapeutic target in their treatment and prevention.

Acknowledgment—We thank Dr. R. Lee for reagents and helpful discussion.

REFERENCES

1. The Diabetes Control and Complications Trial Research Group (1993) The effect of intensive treatment of diabetes on the development and progression of long-term complications in insulin-dependent diabetes mellitus. *N. Engl. J. Med.* **329,** 977–986
2. Molitch, M. E., DeFronzo, R. A., Franz, M. J., Keane, W. F., Mogensen, C. E., Parving, H. H., and Steffes, M. W. (2004) Nephropathy in diabetes. *Diabetes Care* **27,** S79–83
3. Dronavalli, S., Duka, I., and Bakris, G. L. (2008) The pathogenesis of diabetic nephropathy. *Nat. Clin. Pract. Endocrinol. Metab.* **4,** 444–452
4. Kakehi, T., and Yabe-Nishimura, C. (2008) NOX enzymes and diabetic complications. *Semin. Immunopathol.* **30,** 301–314
5. Kanwar, Y. S., Wada, J., Sun, L., Xie, P., Wallner, E. I., Chen, S., Chugh, S., and Danesh, F. R. (2008) Diabetic nephropathy. Mechanisms of renal disease progression. *Exp. Biol. Med.* **233,** 4–11
6. Lee, H. B., Yu, M. R., Yang, Y., Jiang, Z., and Ha, H. (2003) Reactive oxygen species-regulated signaling pathways in diabetic nephropathy. *J. Am. Soc. Nephrol.* **14,** S241–245
7. Kobayashi, T., Uehara, S., Ikeda, T., Itadani, H., and Kotani, H. (2003) Vitamin D_3 up-regulated protein-1 regulates collagen expression in mesangial cells. *Kidney Int.* **64,** 1632–1642
8. Shankland, S. J. (2006) The podocyte's response to injury. Role in proteinuria and glomerulosclerosis. *Kidney Int.* **69,** 2131–2147
9. Brownlee, M. (2005) The pathobiology of diabetic complications. A unifying mechanism. *Diabetes* **54,** 1615–1625

10. Nishikawa, T., Edelstein, D., Du, X. L., Yamagishi, S., Matsumura, T., Kaneda, Y., Yorek, M. A., Beebe, D., Oates, P. J., Hammes, H. P., Giardino, I., and Brownlee, M. (2000) Normalizing mitochondrial superoxide production blocks three pathways of hyperglycaemic damage. *Nature* **404,** 787–790
11. Giacco, F., and Brownlee, M. (2010) Oxidative stress and diabetic complications. *Circ. Res.* **107,** 1058–1070
12. Forbes, J. M., Coughlan, M. T., and Cooper, M. E. (2008) Oxidative stress as a major culprit in kidney disease in diabetes. *Diabetes* **57,** 1446–1454
13. Xia, L., Wang, H., Goldberg, H. J., Munk, S., Fantus, I. G., and Whiteside, C. I. (2006) Mesangial cell NADPH oxidase up-regulation in high glucose is protein kinase C dependent and required for collagen IV expression. *Am. J. Physiol. Renal Physiol.* **290,** F345–356
14. Gorin, Y., Block, K., Hernandez, J., Bhandari, B., Wagner, B., Barnes, J. L., and Abboud, H. E. (2005) Nox4 NAD(P)H oxidase mediates hypertrophy and fibronectin expression in the diabetic kidney. *J. Biol. Chem.* **280,** 39616–39626
15. Thallas-Bonke, V., Thorpe, S. R., Coughlan, M. T., Fukami, K., Yap, F. Y., Sourris, K. C., Penfold, S. A., Bach, L. A., Cooper, M. E., and Forbes, J. M. (2008) Inhibition of NADPH oxidase prevents advanced glycation end product-mediated damage in diabetic nephropathy through a protein kinase C-α-dependent pathway. *Diabetes* **57,** 460–469
16. Block, K., Gorin, Y., and Abboud, H. E. (2009) Subcellular localization of Nox4 and regulation in diabetes. *Proc. Natl. Acad. Sci. U.S.A.* **106,** 14385–14390
17. Chacko, B. K., Reily, C., Srivastava, A., Johnson, M. S., Ye, Y., Ulasova, E., Agarwal, A., Zinn, K. R., Murphy, M. P., Kalyanaraman, B., and Darley-Usmar, V. (2010) Prevention of diabetic nephropathy in Ins2(+/)(AkitaJ) mice by the mitochondria-targeted therapy MitoQ. *Biochem. J.* **432,** 9–19
18. Fujita, H., Fujishima, H., Chida, S., Takahashi, K., Qi, Z., Kanetsuna, Y., Breyer, M. D., Harris, R. C., Yamada, Y., and Takahashi, T. (2009) Reduction of renal superoxide dismutase in progressive diabetic nephropathy. *J. Am. Soc. Nephrol.* **20,** 1303–1313
19. Hamada, Y., Miyata, S., Nii-Kono, T., Kitazawa, R., Kitazawa, S., Higo, S., Fukunaga, M., Ueyama, S., Nakamura, H., Yodoi, J., Fukagawa, M., and Kasuga, M. (2007) Overexpression of thioredoxin1 in transgenic mice suppresses development of diabetic nephropathy. *Nephrol. Dial. Transplant.* **22,** 1547–1557
20. Sedeek, M., Callera, G., Montezano, A., Gutsol, A., Heitz, F., Szyndralewiez, C., Page, P., Kennedy, C. R., Burns, K. D., Touyz, R. M., and Hébert, R. L. (2010) Critical role of Nox4-based NADPH oxidase in glucose-induced oxidative stress in the kidney. Implications in type 2 diabetic nephropathy. *Am. J. Physiol. Renal Physiol.* **299,** F1348–1358
21. Cheng, D. W., Jiang, Y., Shalev, A., Kowluru, R., Crook, E. D., and Singh, L. P. (2006) An analysis of high glucose and glucosamine-induced gene expression and oxidative stress in renal mesangial cells. *Arch. Physiol. Biochem.* **112,** 189–218
22. Parikh, H., Carlsson, E., Chutkow, W. A., Johansson, L. E., Storgaard, H., Poulsen, P., Saxena, R., Ladd, C., Schulze, P. C., Mazzini, M. J., Jensen, C. B., Krook, A., Björnholm, M., Tornqvist, H., Zierath, J. R., Ridderstråle, M., Altshuler, D., Lee, R. T., Vaag, A., Groop, L. C., and Mootha, V. K. (2007) TXNIP regulates peripheral glucose metabolism in humans. *PLoS Med.* **4,** e158
23. Shalev, A., Pise-Masison, C. A., Radonovich, M., Hoffmann, S. C., Hirshberg, B., Brady, J. N., and Harlan, D. M. (2002) Oligonucleotide microarray analysis of intact human pancreatic islets. Identification of glucose-responsive genes and a highly regulated TGFβ signaling pathway. *Endocrinology* **143,** 3695–3698
24. Chen, K. S., and DeLuca, H. F. (1994) Isolation and characterization of a novel cDNA from HL-60 cells treated with 1,25-dihydroxyvitamin D_3. *Biochim. Biophys. Acta* **1219,** 26–32
25. Miranda-Vizuete, A., Damdimopoulos, A. E., Gustafsson, J., and Spyrou, G. (1997) Cloning, expression, and characterization of a novel *Escherichia coli* thioredoxin. *J. Biol. Chem.* **272,** 30841–30847
26. Patwari, P., Higgins, L. J., Chutkow, W. A., Yoshioka, J., and Lee, R. T. (2006) The interaction of thioredoxin with TxNIP. Evidence for formation of a mixed disulfide by disulfide exchange. *J. Biol. Chem.* **281,** 21884–21891
27. Schulze, P. C., Yoshioka, J., Takahashi, T., He, Z., King, G. L., and Lee, R. T. (2004) Hyperglycemia promotes oxidative stress through inhibition of thioredoxin function by thioredoxin-interacting protein. *J. Biol. Chem.* **279,** 30369–30374
28. Masson, E., Koren, S., Razik, F., Goldberg, H., Kwan, E. P., Sheu, L., Gaisano, H. Y., and Fantus, I. G. (2009) High β-cell mass prevents streptozotocin-induced diabetes in thioredoxin-interacting protein-deficient mice. *Am. J. Physiol. Endocrinol. Metab.* **296,** E1251–1261
29. Chen, J., Hui, S. T., Couto, F. M., Mungrue, I. N., Davis, D. B., Attie, A. D., Lusis, A. J., Davis, R. A., and Shalev, A. (2008) Thioredoxin-interacting protein deficiency induces Akt/Bcl-xL signaling and pancreatic β-cell mass and protects against diabetes. *FASEB J.* **22,** 3581–3594
30. Chen, J., Fontes, G., Saxena, G., Poitout, V., and Shalev, A. (2010) Lack of TxNIP protects against mitochondria-mediated apoptosis but not against fatty acid-induced ER stress-mediated β-cell death. *Diabetes* **59,** 440–447
31. Minn, A. H., Hafele, C., and Shalev, A. (2005) Thioredoxin-interacting protein is stimulated by glucose through a carbohydrate response element and induces β-cell apoptosis. *Endocrinology* **146,** 2397–2405
32. Menè, P., and Stoppacciaro, A. (2009) Isolation and propagation of glomerular mesangial cells. *Methods Mol. Biol.* **466,** 3–17
33. Takemoto, M., Asker, N., Gerhardt, H., Lundkvist, A., Johansson, B. R., Saito, Y., and Betsholtz, C. (2002) A new method for large scale isolation of kidney glomeruli from mice. *Am. J. Pathol.* **161,** 799–805
34. Beard, K. M., Lu, H., Ho, K., and Fantus, I. G. (2006) Bradykinin augments insulin-stimulated glucose transport in rat adipocytes via endothelial nitric-oxide synthase-mediated inhibition of Jun NH_2-terminal kinase. *Diabetes* **55,** 2678–2687
35. Livak, K. J., and Schmittgen, T. D. (2001) Analysis of relative gene expression data using real-time quantitative PCR and the $2(-\delta\delta\ C_T)$ method. *Methods* **25,** 402–408
36. Chen, J., Chen, J. K., Nagai, K., Plieth, D., Tan, M., Lee, T. C., Threadgill, D. W., Neilson, E. G., and Harris, R. C. (2012) EGFR signaling promotes TGFβ-dependent renal fibrosis. *J. Am. Soc. Nephrol.* **23,** 215–224
37. Li, Y., and Trush, M. A. (1998) Diphenyleneiodonium, an NAD(P)H oxidase inhibitor, also potently inhibits mitochondrial reactive oxygen species production. *Biochem. Biophys. Res. Commun.* **253,** 295–299
38. Björnstedt, M., Kumar, S., and Holmgren, A. (1995) Selenite and selenodiglutathione. Reactions with thioredoxin systems. *Methods Enzymol.* **252,** 209–219
39. Zitman-Gal, T., Green, J., Pasmanik-Chor, M., Oron-Karni, V., and Bernheim, J. (2010) Endothelial pro-atherosclerotic response to extracellular diabetic-like environment. Possible role of thioredoxin-interacting protein. *Nephrol. Dial. Transplant.* **25,** 2141–2149
40. Chen, J., Saxena, G., Mungrue, I. N., Lusis, A. J., and Shalev, A. (2008) Thioredoxin-interacting protein. A critical link between glucose toxicity and β-cell apoptosis. *Diabetes* **57,** 938–944
41. Cha-Molstad, H., Saxena, G., Chen, J., and Shalev, A. (2009) Glucose-stimulated expression of TxNIP is mediated by carbohydrate response element-binding protein, p300, and histone H4 acetylation in pancreatic β cells. *J. Biol. Chem.* **284,** 16898–16905
42. Bodnar, J. S., Chatterjee, A., Castellani, L. W., Ross, D. A., Ohmen, J., Cavalcoli, J., Wu, C., Dains, K. M., Catanese, J., Chu, M., Sheth, S. S., Charugundla, K., Demant, P., West, D. B., de Jong, P., and Lusis, A. J. (2002) Positional cloning of the combined hyperlipidemia gene *Hyplip1*. *Nat. Genet.* **30,** 110–116
43. Balakumar, P., Arora, M. K., Reddy, J., and Anand-Srivastava, M. B. (2009) Pathophysiology of diabetic nephropathy. Involvement of multifaceted signalling mechanism. *J. Cardiovasc. Pharmacol.* **54,** 129–138
44. Spencer, N. Y., Yan, Z., Boudreau, R. L., Zhang, Y., Luo, M., Li, Q., Tian, X., Shah, A. M., Davisson, R. L., Davidson, B., Banfi, B., and Engelhardt, J. F. (2011) Control of hepatic nuclear superoxide production by glucose-6-phosphate dehydrogenase and NADPH oxidase-4. *J. Biol. Chem.* **286,** 8977–8987
45. Lambeth, J. D., Kawahara, T., and Diebold, B. (2007) Regulation of Nox and Duox enzymatic activity and expression. *Free Radic. Biol. Med.* **43,** 319–331
46. Kitada, M., Koya, D., Sugimoto, T., Isono, M., Araki, S., Kashiwagi, A., and Haneda, M. (2003) Translocation of glomerular p47phox and p67phox by

protein kinase C-β activation is required for oxidative stress in diabetic nephropathy. *Diabetes* **52,** 2603–2614
47. Li, J., Zhu, H., Shen, E., Wan, L., Arnold, J. M., and Peng, T. (2010) Deficiency of rac1 blocks NADPH oxidase activation, inhibits endoplasmic reticulum stress, and reduces myocardial remodeling in a mouse model of type 1 diabetes. *Diabetes* **59,** 2033–2042
48. Martyn, K. D., Frederick, L. M., von Loehneysen, K., Dinauer, M. C., and Knaus, U. G. (2006) Functional analysis of Nox4 reveals unique characteristics compared with other NADPH oxidases. *Cell Signal.* **18,** 69–82
49. Serrander, L., Cartier, L., Bedard, K., Banfi, B., Lardy, B., Plastre, O., Sienkiewicz, A., Fórró, L., Schlegel, W., and Krause, K. H. (2007) NOX4 activity is determined by mRNA levels and reveals a unique pattern of ROS generation. *Biochem. J.* **406,** 105–114
50. Yoshioka, J., Chutkow, W. A., Lee, S., Kim, J. B., Yan, J., Tian, R., Lindsey, M. L., Feener, E. P., Seidman, C. E., Seidman, J. G., and Lee, R. T. (2012) Deletion of thioredoxin-interacting protein in mice impairs mitochondrial function but protects the myocardium from ischemia-reperfusion injury. *J. Clin. Invest.* **122,** 267–279
51. Perry, S. W., Norman, J. P., Barbieri, J., Brown, E. B., and Gelbard, H. A. (2011) Mitochondrial membrane potential probes and the proton gradient. A practical usage guide. *BioTechniques* **50,** 98–115
52. Mathur, A., Hong, Y., Kemp, B. K., Barrientos, A. A., and Erusalimsky, J. D. (2000) Evaluation of fluorescent dyes for the detection of mitochondrial membrane potential changes in cultured cardiomyocytes. *Cardiovasc. Res.* **46,** 126–138
53. Singh, D. K., Winocour, P., and Farrington, K. (2011) Oxidative stress in early diabetic nephropathy. Fueling the fire. *Nat. Rev. Endocrinol.* **7,** 176–184
54. Li, X., Rong, Y., Zhang, M., Wang, X. L., LeMaire, S. A., Coselli, J. S., Zhang, Y., and Shen, Y. H. (2009) Up-regulation of thioredoxin interacting protein (TxNIP) by p38 MAPK and FOXO1 contributes to the impaired thioredoxin activity and increased ROS in glucose-treated endothelial cells. *Biochem. Biophys. Res. Commun.* **381,** 660–665
55. Zhang, L., Sheppard, O. R., Shah, A. M., and Brewer, A. C. (2008) Positive regulation of the NADPH oxidase NOX4 promoter in vascular smooth muscle cells by E2F. *Free Radic. Biol. Med.* **45,** 679–685
56. Manea, A., Tanase, L. I., Raicu, M., and Simionescu, M. (2010) Transcriptional regulation of NADPH oxidase isoforms, Nox1 and Nox4, by nuclear factor-κB in human aortic smooth muscle cells. *Biochem. Biophys. Res. Commun.* **396,** 901–907
57. Manea, A., Manea, S. A., Gafencu, A. V., Raicu, M., and Simionescu, M. (2008) AP-1-dependent transcriptional regulation of NADPH oxidase in human aortic smooth muscle cells. Role of p22phox subunit. *Arterioscler. Thromb. Vasc. Biol.* **28,** 878–885
58. Diebold, I., Petry, A., Hess, J., and Görlach, A. (2010) The NADPH oxidase subunit NOX4 is a new target gene of the hypoxia-inducible factor-1. *Mol. Biol. Cell* **21,** 2087–2096
59. Pendyala, S., Moitra, J., Kalari, S., Kleeberger, S. R., Zhao, Y., Reddy, S. P., Garcia, J. G., and Natarajan, V. (2011) Nrf2 regulates hyperoxia-induced Nox4 expression in human lung endothelium. Identification of functional antioxidant response elements on the Nox4 promoter. *Free Radic. Biol. Med.* **50,** 1749–1759
60. He, X., Kan, H., Cai, L., and Ma, Q. (2009) Nrf2 is critical in defense against high glucose-induced oxidative damage in cardiomyocytes. *J. Mol. Cell Cardiol.* **46,** 47–58
61. Zhang, R., Al-Lamki, R., Bai, L., Streb, J. W., Miano, J. M., Bradley, J., and Min, W. (2004) Thioredoxin-2 inhibits mitochondria-located ASK1-mediated apoptosis in a JNK-independent manner. *Circ. Res.* **94,** 1483–1491
62. Fujino, G., Noguchi, T., Matsuzawa, A., Yamauchi, S., Saitoh, M., Takeda, K., and Ichijo, H. (2007) Thioredoxin and TRAF family proteins regulate reactive oxygen species-dependent activation of ASK1 through reciprocal modulation of the N-terminal homophilic interaction of ASK1. *Mol. Cell Biol.* **27,** 8152–8163
63. Hattori, K., Naguro, I., Runchel, C., and Ichijo, H. (2009) The roles of ASK family proteins in stress responses and diseases. *Cell Commun. Signal.* **7,** 9
64. Yamawaki, H., Pan, S., Lee, R. T., and Berk, B. C. (2005) Fluid shear stress inhibits vascular inflammation by decreasing thioredoxin-interacting protein in endothelial cells. *J. Clin. Invest.* **115,** 733–738
65. Saxena, G., Chen, J., and Shalev, A. (2010) Intracellular shuttling and mitochondrial function of thioredoxin-interacting protein. *J. Biol. Chem.* **285,** 3997–4005
66. Chen, C. L., Lin, C. F., Chang, W. T., Huang, W. C., Teng, C. F., and Lin, Y. S. (2008) Ceramide induces p38 MAPK and JNK activation through a mechanism involving a thioredoxin-interacting protein-mediated pathway. *Blood* **111,** 4365–4374
67. Lv, Z. M., Wang, Q., Wan, Q., Lin, J. G., Hu, M. S., Liu, Y. X., and Wang, R. (2011) The role of the p38 MAPK signaling pathway in high glucose-induced epithelial-mesenchymal transition of cultured human renal tubular epithelial cells. *PLoS One* **6,** e22806
68. Lan, T., Liu, W., Xie, X., Xu, S., Huang, K., Peng, J., Shen, X., Liu, P., Wang, L., Xia, P., and Huang, H. (2011) Sphingosine kinase-1 pathway mediates high glucose-induced fibronectin expression in glomerular mesangial cells. *Mol. Endocrinol.* **25,** 2094–2105
69. Gloire, G., Legrand-Poels, S., and Piette, J. (2006) NF-κB activation by reactive oxygen species. Fifteen years later. *Biochem. Pharmacol.* **72,** 1493–1505
70. Yang, W. S., Seo, J. W., Han, N. J., Choi, J., Lee, K. U., Ahn, H., Lee, S. K., and Park, S. K. (2008) High glucose-induced NF-κB activation occurs via tyrosine phosphorylation of IκBα in human glomerular endothelial cells. Involvement of Syk tyrosine kinase. *Am. J. Physiol. Renal Physiol.* **294,** F1065–1075
71. Li, H., Wang, F., Zhang, L., Cao, Y., Liu, W., Hao, J., Liu, Q., and Duan, H. (2011) Modulation of Nrf2 expression alters high glucose-induced oxidative stress and antioxidant gene expression in mouse mesangial cells. *Cell Signal.* **23,** 1625–1632
72. Patwari, P., Chutkow, W. A., Cummings, K., Verstraeten, V. L., Lammerding, J., Schreiter, E. R., and Lee, R. T. (2009) Thioredoxin-independent regulation of metabolism by the α-arrestin proteins. *J. Biol. Chem.* **284,** 24996–25003
73. Jeon, J. H., Lee, K. N., Hwang, C. Y., Kwon, K. S., You, K. H., and Choi, I. (2005) Tumor suppressor VDUP1 increases $p27^{kip1}$ stability by inhibiting JAB1. *Cancer Res.* **65,** 4485–4489
74. Zhou, R., Tardivel, A., Thorens, B., Choi, I., and Tschopp, J. (2010) Thioredoxin-interacting protein links oxidative stress to inflammasome activation. *Nat. Immunol.* **11,** 136–140
75. Lee, S., Kim, S. M., and Lee, R. T. (2012) Thioredoxin and thioredoxin target proteins. From molecular mechanisms to functional significance. *Antioxid. Redox Signal.* 10.1089/ARS. 2011.4322